4. J.R. James and P.S. Hall, Handbook of microstrip antennas, IEE Electromagnetic Wave Series No. 28, Peter Peregrinus, London, Vols. 1 and 2, 1989.
5. Y.T. Lo, S.M. Wright, and M. Davidovitz, Microstrip Antennas, In: K. Chang (Ed.), Handbook of microwave and optical components, Vol. 1, Wiley, New York, 1989, pp. 764–889.
6. D.M. Pozar and D.H. Schaubert (Eds.), Microstrip antennas—The analysis and design of microstrip antennas and arrays, IEEE Press, New York, 1995.
7. R. Garg, P. Bhartia, I. Bahl, and A. Ittipiboon, Microstrip antenna design handbook, Artech House, Canton, MA, 2001.
8. I. Wolff and N. Knoppik, Rectangular and circular microstrip disc capacitors and resonators, IEEE Trans Microwave Theory Tech MTT-22 (1974), 857–864.
9. W.C. Chew and J.A. Kong, Effects of fringing fields on the capacitance of circular microstrip disk, IEEE Trans Microwave Theory Tech MTT-28 (1980), 98–104.
10. W.C. Chew and J.A. Kong, Analysis of a circular microstrip disk antenna with a thick dielectric substrate, IEEE Trans Antennas Propagat AP-29 (1981), 68–76.
11. T. Itoh and R. Mittra, Analysis of a microstrip disk resonator, AEU Int J Electron Commun 27 (1973), 456–458.
12. J.Q. Howell, Microstrip antennas, IEEE Trans Antennas Propagat AP-23 (1975), 90–93.
13. S.A. Long, L.C. Shen, M.D. Walton, and M.R. Allerding, Impedance of a circular disk printed- circuit antenna, Electron Lett 14 (1978), 684–686.
14. K.R. Carver, Practical analytical techniques for the microstrip antenna, Proc Workshop Printed Circ Antenna Technol, Las Cruces, New Mexico, 1979, pp. 7.1–7.20.
15. S. Yano and A. Ishimaru, A theoretical study of the input impedance of a circular microstrip disk antenna, IEEE Trans Antennas Propagat AP-29 (1981), 77–83.
16. J.S. Dahele and K.F. Lee, Effect of substrate thickness on the performance of a circular-disk microstrip antenna, IEEE Trans Antennas Propagat AP-31 (1983), 358–360.
17. J.S. Dahele and K.F. Lee, Theory and experiment on microstrip antenna with air gaps, IEE Proc PtH 32 (1985), 455–460.
18. M. Davidovitz and Y.T. Lo, Input impedance of a probe-fed circular microstrip antenna with thick substrate, IEEE Trans Antennas Propagat AP-34 (1986), 905–911.
19. F. Abboud, J.P. Damiano, and A. Papiernik, New determination of resonant frequency of circular disc microstrip antenna: application to thick substrate, Electron Lett 24 (1988), 1104–1106.
20. K. Antoszkiewicz and L. Shafai, Impedance characteristics of circular microstrip patches, IEEE Trans Antennas Propagat AP-38 (1990), 942–946.
21. V. Losada, R.R. Boix, and M. Horno, Resonant modes of circular microstrip patches in multilayered substrates, IEEE Trans Microwave Theory Tech MTT-47 (1999), 488–497.
22. K.F. Lee and Z. Fan, CAD formulas for resonant frequencies of TM_{11} mode of circular patch antenna with or without superstrate, Microwave Opt Technol Lett 7 (1994), 570–573.
23. N. Kumprasert and W. Kiranon, Simple and accurate formula for the resonant frequency of the circular microstrip disk antenna, IEEE Trans Antennas Propagat AP-43 (1995), 1331–1333.
24. J.S. Roy and B. Jecko, A formula for the resonance frequencies of circular microstrip patch antennas satisfying CAD requirements, Int J RF Microwave Comp Aided Eng 3 (1993), 67–70.
25. Q. Liu and W.C. Chew, Curve-fitting formulas for fast determination of accurate resonant frequency of circular microstrip patches, IEE Proc Microwave Antennas Propagat PtH 135 (1988), 289–292.
26. N. Karaboga, K. Guney, and A. Akdagli, A new effective patch radius expression obtained by using a modified tabu search algorithm for the resonant frequency of electrically thick circular microstrip antennae, Int J Electron 86 (1999), 825–835.
27. A. Akdagli and K. Guney, Effective patch radius expression obtained using a genetic algorithm for the resonant frequency of electrically thin and thick circular microstrip antennas, IEE Proc Microwave Antennas Propagat PtH 147 (2000), 156–159.
28. C.S. Gurel and E. Yazgan, New determination of dynamic permittivity and resonant frequency of tunable circular disk microstrip structures, Int J RF Microwave Comp Aided Eng 10 (2000), 120–126.
29. R. Storn and K. Price, Differential evolution—A simple and efficient heuristic for global optimization over continuous spaces, J Global Optimizat 11 (1997), 341–359.
30. K.A. Michalski, Electromagnetic imaging of elliptical cylindrical conductors and tunnels using a differential evolution algorithm, Microwave Opt Technol Lett 28 (2001), 164–169.
31. A. Qing, Electromagnetic inverse scattering of multiple two-dimensional perfectly conducting objects by the differential evolution strategy, IEEE Trans Antennas Propagat AP-51 (2003), 1251–1262.
32. X.F. Luo, A. Qing, and C.K. Lee, Application of the differential-evolution strategy to the design of frequency-selective surfaces, Int J RF Microwave Comp Aided Eng 15 (2005), 173–180.
33. A. Akdagli and M.E. Yuksel, Application of differential evolution algorithm to the modeling of laser diode nonlinearity in a radio-overfiber network, Microwave Opt Technol Lett 48 (2006), 1130–1133.
34. C. Yildiz, A. Akdagli, and M. Turkmen, Simple and accurate synthesis formulas obtained by using a differential evolution algorithm for coplanar striplines, Microwave Opt Technol Lett 48 (2006), 1133–1137.

SMALL SIZE STEPPED IMPEDANCE LOW PASS FILTERS

Ashraf S. Mohra and Majeed A. Alkanhal
Department of Electrical Engineering, King Saud University, P.O. Box: 800, Riyadh 11421, Saudi Arabia; Corresponding author: amohra@ksu.edu.sa or ashraf_mohra@yahoo.com

Received 3 March 2007

ABSTRACT: *A reduction in the overall size of the stepped impedance low pass filter is proposed in this article. The high impedance line sections are converted to T-sections and the low impedance line sections are converted to π-sections. Analysis and design equations for such conversions are presented. This method accomplishes a prominent size reduction in sharp response filters with multi-stepped impedance sections.* © 2007 Wiley Periodicals, Inc. Microwave Opt Technol Lett 49: 2398–2403, 2007; Published online in Wiley InterScience (www.interscience.wiley.com). DOI 10.1002/mop.22766

Key words: *microstrip filters; stepped impedance; compact filters; size reduction*

1. INTRODUCTION

The use of microwave filters can be found in many applications in microwave circuits and telecommunication systems such as radar, satellite, mobile communications systems. Such systems often require circuits to be as small as possible and implemented in low profile topologies such as microstrip lines, slot lines, and coplanar waveguides. Microstrip is one of the dominant technologies, which can provide size reduction for microwave circuits. The stepped impedance filter is one of the conventional filters, mainly due to the ease of implementation in either microstrip or coplanar technology. This filter is normally composed of alternating low and high impedance regions (the high impedance lines act as series inductors and the low impedance lines act as shunt capacitors), where the change in impedance is controlled by the width of the strip. For achieving a high degree of attenuation in the stop band it is necessary to obtain a high to low impedance ratio (Z_{oH}/Z_{oL}) or

to increase the order of the filter. Also, one of the main requirements for the stepped impedance filter is that each section must be less than half of the quarter wavelength at the cutoff frequency ($l < \lambda/8$). The overall size of the filter will be large at low frequencies especially if the number of the elements is increased to achieve special requirements as in sharp edge filters.

In this article, we propose a reduction in the overall size of the stepped impedance filter by transferring the high impedance filter sections into compact T-sections and transferring the low impedance filter sections into compact Π-sections. Analysis of each of the T-section and Π-section equivalence is illustrated in Sections 2 and 3, respectively. Basic theory of the stepped impedance low pass filters is given in Section 4. A five-section Chebyshev low pass filter design with 25% size reduction is investigated. The designed filter is realized using microstrip technology and then measured by Vector network analyzer. The measured S-parameters of the realized Chebyshev stepped impedance filters is compared with the simulated results in Section 5. A very good agreement between experimental and simulation results is confirmed. The proposed technique achieves, even, more substantial size reduction in sharp response filters with multi-stepped impedance sections.

2. EQUIVALENT T-SHAPED TRANSMISSION LINE SECTION

The T-shaped transmission line model is consisted of two identical series transmission lines and one shunt open stub located in the center of the two series lines as shown in Figure 1. The equivalence between the high impedance transmission line sections and the T-section is investigated utilizing the ABCD matrices for both networks. Refs. 1 and 2 presented analysis of the equivalence of a transmission line sections to T-sections but their analysis was limited to transmission line sections with electrical length equal to quarter wavelength only. Here we presented general analysis for

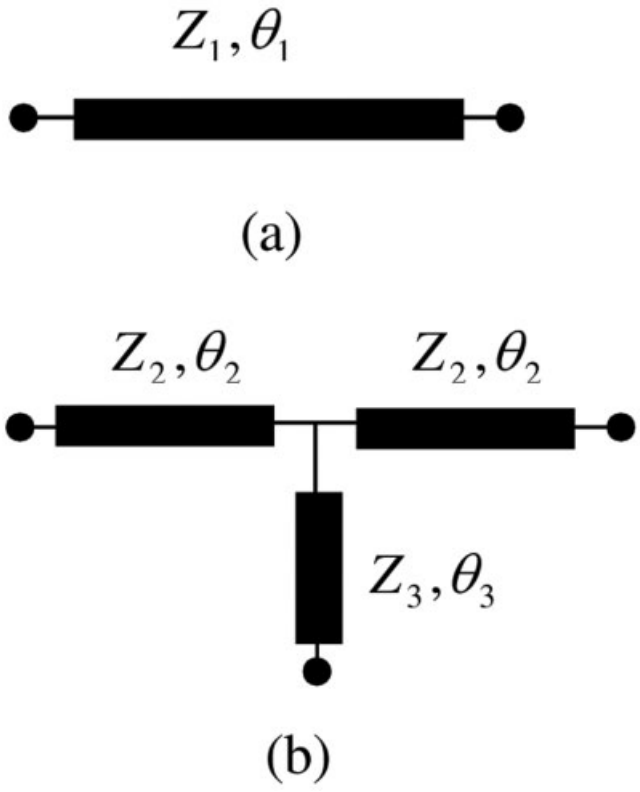

Figure 1 (a) Transmission line section and (b) T-equivalent section

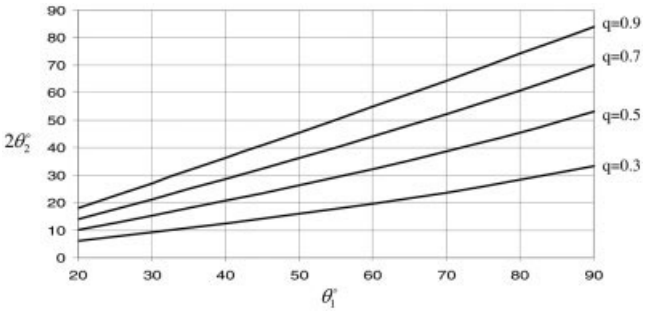

Figure 2 The variation of electrical length $2\theta_2$ against θ_1 at different impedance ratio q

any length less than or equal to quarter wavelength ($l \leq \lambda/4$). The ABCD matrix for the original transmission line of Figure 1(a), is

$$M_1 = \begin{bmatrix} \cos\theta_1 & jz_1 \sin\theta_1 \\ jy_1 \sin\theta_1 & \cos\theta_1 \end{bmatrix} \tag{1}$$

The ABCD matrix for the T-shaped transmission line section of Figure 1(b) is

$$M_T = M_2 M_3 M_2 \tag{2}$$

where M_2, the ABCD matrix for the series elements, is given by

$$M_2 = \begin{bmatrix} \cos\theta_2 & jz_2 \sin\theta_2 \\ jy_2 \sin\theta_2 & \cos\theta_2 \end{bmatrix} \tag{3}$$

and M_3, the ABCD matrix for the shunt open stub, is given by

$$M_3 = \begin{bmatrix} 1 & 0 \\ jy_3 \tan\theta_3 & 1 \end{bmatrix} \tag{4}$$

Equating the ABCD matrix of Eq. (1) and the ABCD matrix of Eq. (2), the relations between the electrical lengths of the main transmission line and the equivalent T-section are obtained as follows:

$$\theta_1 = \cos^{-1}\left\{\cos(2\theta_2) - \frac{(1-q^2)\sin^2(2\theta_2)}{2[q^2\cos^2\theta_2 + \sin^2\theta_2]}\right\} \tag{5}$$

$$\theta_3 = \tan^{-1}\left\{\frac{q(1-q^2)\sin(2\theta_2)}{r[q^2\cos^2\theta_2 + \sin^2\theta_2]}\right\} \tag{6}$$

where q and r are impedance ratios given by:

$$q = (z_1/z_2), \quad r = (z_1/z_3) \tag{7}$$

Equation (5) is solved by iteration. The variation of electrical length $2\theta_2$ against θ_1 at different values of the impedance ratio q is illustrated in Figure 2. As the electrical length θ_2 is determined, the electrical length θ_3 can be calculated directly from Eq. (6) with proper impedance ratio r. From Figure 2, as an illustration, if we chose $q = 0.5$, the electrical length for a transmission line θ_1 can be reduced from $\theta_1 = 50°$ to an electrical length $2\theta_2 = 26°$, which is a noticeable 48% reduction in size. As the impedance ratios q and r are increased (but $q < 1$), the electrical length θ_3 will be smaller. When $q = 1$, the electrical length $2\theta_2$ is equal to θ_1 and in this case the electrical length θ_3 is zero, which means that there is no conversion to T-section occurs. For practical implementation,

it is necessary to take into consideration that the width corresponding to Z_3 must be less than the electrical length $2\theta_2$. Therefore, the practical range for impedance ratios q and r is defined as ($0.3 < q < 1.0$ and $0.3 < r < 4.0$).

3. EQUIVALENT Π -SHAPED TRANSMISSION LINE SECTION

Another method to reduce the size of a transmission line is the conversion to equivalent Π -shaped sections. The Π -shaped sections consists of a series element and two shunt open stubs as shown in Figure 3. ABCD matrix are used to transfer the original transmission line sections to its Π -equivalent section.

The ABCD matrix for the original transmission line is the same as in Eq. (1), while the ABCD matrix for the Π -shaped transmission line section is given by:

$$M_\pi = M_3 M_2 M_3 \tag{8}$$

where M_2 the ABCD matrix for the series element is given by

$$M_2 = \begin{bmatrix} \cos\theta_2 & jz_2 \sin\theta_2 \\ jy_2 \sin\theta_2 & \cos\theta_2 \end{bmatrix} \tag{9}$$

and M_3, the ABCD matrix for each of the shunt opens stubs elements, is given by

$$M_3 = \begin{bmatrix} 1 & 0 \\ jy_3 \tan\theta_3 & 1 \end{bmatrix} \tag{10}$$

Equating the individual elements of the ABCD matrices of Eqs. (1) and (8), the electrical lengths of the equivalent Π-shaped section are as follows:

$$\theta_2 = \sin^{-1}(p \sin\theta_1) \tag{11}$$

$$\theta_3 = \tan^{-1}\left\{\frac{p(\cos\theta_2 - \cos\theta_1)}{k \sin\theta_2}\right\} \tag{12}$$

where p and q are impedance ratios given by

$$p = (z_1/z_2), \quad k = (z_1/z_3) \tag{13}$$

with the proper value for the impedance ratio p, the electrical length θ_2 can be calculated from Eq. (11). Also, with proper value for the impedance ratio k, the value of the electrical length θ_3 can be calculated from Eq. (12). Figure 4 illustrates the variation of electrical length θ_2 against θ_1 at different values of impedance ratio p. The impedance ratio p must be less than 1 to make Eq. (11) useful. When $p = 1$ and $k = 1$, then $\theta_2 = \theta_1$ and $\theta_3 = 0$, which implies that there is no conversion occurred. Also, as the impedance ratio p decreases, the electrical length θ_2 will be smaller with respect to θ_1 while the electrical length θ_3 will be larger. Thus, to compensate for the increase of the electrical length θ_3, the impedance ratio k must be chosen large. Added to that, the corresponding width of Z must be maintained less than the electrical length θ_2 .

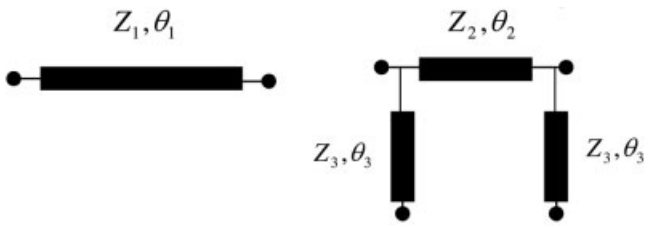

Figure 3 The transmission line and its Π-equivalent

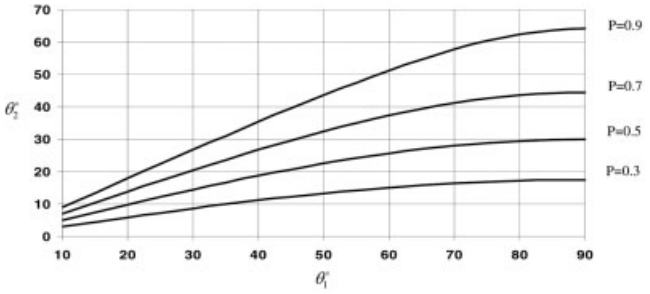

Figure 4 The variation of electrical length θ_2 against θ_1 at different impedance ratio p

4. STEPPED IMPEDANCE LOW PASS FILTER

An efficient way to implement low pass filters in microstrip or stripline geometries is to use alternating sections of very high and very low characteristic impedance lines. Such filters are usually referred as stepped impedance filters. The stepped impedance filters are popular because they are easier to design and take up less space than a similar low-pass filter using stubs. The high impedance sections act as series inductors and the low impedance sections act as shunt capacitor. Expression for these inductance and capacitance depend upon both characteristic impedance and their transmission line lengths. It would be practical to initially fix the characteristic impedances of high and low impedance lines by the following considerations presented in [3]:

- $Z_{oC} < Z_o < Z_{oL}$, where Z_{oC} and Z_{oL} denote the characteristic impedances corresponding to shunt capacitance and series inductance respectively, and Z_o is the source impedance usually 50 Ω for microstrip lines.
- Lower Z_{oC} results in a better approximation of lumped-element capacitor, but the resulting wide line width W_C must not allow any transverse resonance to occur at operating frequencies.
- Higher Z_{oL} leads to a better approximation of a lumped inductor element, but Z_{oL} must not be so high that the transmission line fabrication becomes inordinately difficult or its current carrying capability becomes a limitation.

The electrical length corresponding to inductor and capacitor sections can be calculated [4] as:

$$(\beta l)_{\text{inductor}} = \frac{LZ_o}{Z_{oL}} \tag{14}$$

$$(\beta l)_{\text{icapacitor}} = \frac{CZ_{oC}}{Z_o} \tag{15}$$

where Z_o is the filter impedance which is normally 50 Ω while L and C are the normalized element values. The details of specifying low pass Butterworth and Chebyshev filter are presented next.

4.1 Butterworth Low Pass Prototype Filter

The Butterworth response exhibits the maximally flat passband and stopband regions. For Butterworth or maximally flat lowpass prototype filters having an insertion loss $L_{Ar} = 3.01$ dB at the

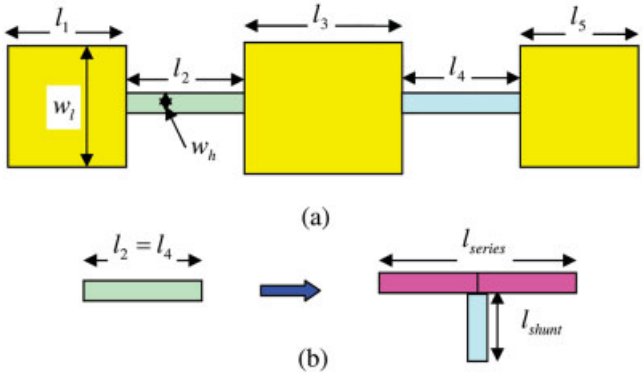

Figure 5 (a) The physical dimensions of the low pass filter. (b) The conversion of high impedance section to its T-shape equivalent. [Color figure can be viewed in the online issue, which is available at www.interscience.wiley.com]

cutoff frequency ($\Omega_c = 1.0$), the element g_k values are given by [3]:

$$g_0 = g_{n+1} = 1 \tag{16}$$

$$g_i = 2\sin\left\{\frac{(2i-1)\pi}{2n}\right\} \quad i = 1 \quad \text{to } n \tag{17}$$

The Butterworth filters considered here is always symmetrical; namely $g_0 = g_{n+1}$ and $g_1 = g_n$ and so on. The degree n of a Butterworth lowpass prototype is given by the following equation [3]:

$$n \geq \frac{\log(10^{0.1L_s} - 1)}{2\log\Omega_s} \tag{18}$$

$$\Omega_s = \frac{\omega_s}{\omega_c} \tag{19}$$

where ω_s is the frequency at which, the filter will achieve certain insertion loss, ω_c is the cutoff frequency of the filter and L_{AS} is the minimum stopped attenuation. For example, if $L_{AS} = 40$ dB and $\Omega_s = 2$, then a Butterworth low pass filter prototype with $n = 7$ should be chosen.

4.2 Chebyshev Low Pass Prototype Filter

The Chebyshev filter exhibits an equal-ripple response in the passband region and maximally flat response in the stopband region. When the passband ripple is L_{Ar} at the cutoff frequency $\Omega_c = 1$ then the g_k elements are [3]:

$$g_o = 1.0 \tag{20}$$

$$g_1 = \frac{2}{\gamma}\sin\left(\frac{\pi}{2n}\right) \tag{21}$$

$$g_i = \frac{1}{g_{(i-1)}} \frac{4\sin\left[\frac{(2i-1)\pi}{2n}\right]\sin\left[\frac{(2i-3)\pi}{2n}\right]}{\gamma^2 + \sin^2\left[\frac{(i-1)\pi}{n}\right]} \quad i = 2,3,\ldots,n \tag{22}$$

$$g_{i+1} = \begin{cases} 1.0 & \text{for } n \text{ odd} \\ \coth^2(\beta/4) & \text{for } n \text{ even} \end{cases} \tag{23}$$

where

$$\beta = \ln\left[\coth\left(\frac{L_{Ar}}{17.37}\right)\right] \tag{24}$$

$$\gamma = \sinh\left(\frac{\beta}{2n}\right) \tag{25}$$

For the required passband ripple (L_{Ar} dB), and the minimum stopband attenuation (L_{As} dB) at $\Omega = \Omega_s$, the degree n of the Chebyshev lowpass prototype can be obtained from [3]:

$$n \geq \frac{\cosh^{-1}\sqrt{\frac{(10^{0.1L_{AS}-1})}{(10^{0.1L_{As}}-1)}}}{\cosh^{-1}\Omega_s} \tag{26}$$

5. COMPACT FILTER DESIGN

In this section, two design cases are presented; the maximally flat and the Chebyshev response low pass filters.

5.1 Maximally Flat Filter

A design for a maximally flat stepped impedance low pass filter was carried out at $f_c = 2$ GHz . The filter has a stopband attenuation of 25 dB at $f = 4.5$ GHz . Utilizing Eqs. (14)–(19), the filter was specified to have five elements and the g_k values are calculated accordingly. The filter was designed on RT/Duroid substrate ($\varepsilon_r = 2.2$, $h = 1.5748$ mm), with the low and high characteristic impedances chosen as 20 and 100 Ω, respectively. The corresponding lengths and widths [Fig. 5(a)] will be$l_1 = l_5 = 3.4$ mm, $l_2 = l_4 = 11.89$ mm, $l_3 = 11.04$ mm, $W_l = 16.2$ *mm*, and $W_h = 1.36$ m . From Eqs. (5)–(7), with $q = 0.8$ and $r = 1$, the two high impedances sections l_2 and l_4 can be converted to their T-section equivalent [Fig. 5(b)] with $l_{series} = 8.34$ mm and $l_{shunt} = 5.615$ mm . The overall length of the stepped impedance low pass filter is then reduced by 17%. Both the original and modified stepped impedance low pass filters are simulated using IE3D software [5], and their S-parameters are illustrated in Figure 6. From the simulated results, it is found that the S-parameters are almost similar. Hence, the reduced size stepped impedance low pass filter has the same properties of the original filter.

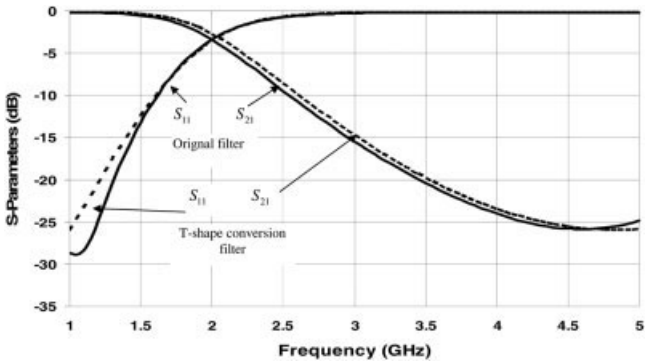

Figure 6 The simulated S-parameters for original stepped impedance low pass filter and the T-shaped equivalent filter

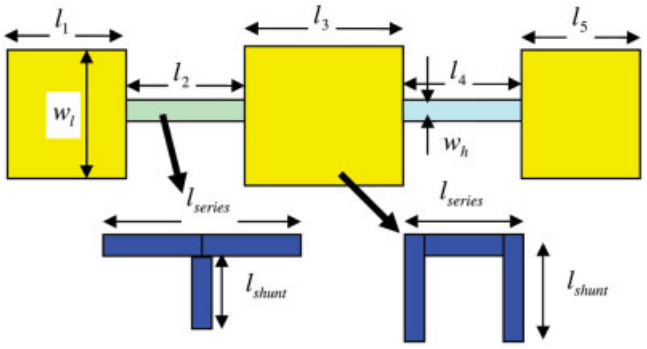

Figure 7 The physical dimensions of the designed Chebyshev low passes filter and sections conversion to T-shaped and Π-shaped sections. [Color figure can be viewed in the online issue, which is available at www.interscience.wiley.com]

5.2 Chebyshev Filter

A design for a Chebyshev stepped impedance low pass filter was carried out at $f_c = 2.25$ GHz . The filter has a stopband attenuation of 25 dB at $f = 5$ GHz with a response has a ripple of 0.1 dB. Using Eqs. (20)–(26), the filter has five elements and then g_k values are calculated accordingly. The filter was designed on RT/Duroid substrate ($\varepsilon_r = 2.2$, $h = 1.5748$ mm), and the low and high characteristic impedances are chosen as 20 and 120 Ω respectively. The corresponding lengths and widths (Fig. 7) will be $l_1 = 7.42$ mm, $l_2 = 9.86$ mm, $l_3 = 11.85$ mm, $l_4 = 6.18$ mm, $l_5 = 9.06$ mm, $W_l = 16.2$ mm, and $W_h = 0.88$ m . The section l_2 was converted to its T-shape equivalent with $q = 0.8$ and $r = 1.0$, this results in, $l_{series} = 8.03$ mm and $l_{shunt} = 3.55$ mm . The section l_3 was converted to its Π -equivalent with $p = k = 0.2$. The Π -equivalent section dimensions are $l_{series} = 2.35$ mm and $l_{shunt} = 19.045$ mm . The overall length of the modified low pass stepped impedance filter is reduced by 25%. Both the original stepped impedance low pass filter and the compact are simulated using IE3D software [5], and their S-parameters are shown in Figure 8. It is found that, the reflection parameter S_{11} has the same response for both filters types. The transmission parameter S_{21} for the reduced size filter is better in the band (0.5–3.6 GHz) while it has less performance in the band (3.6–5 GHz), but it still has an accepted value less than (−20 dB). The cutoff frequency is slightly shifted by 0.05 GHz for both filter types. Such slight shift can be compensated by slight increase in the length of one of the outer sections.

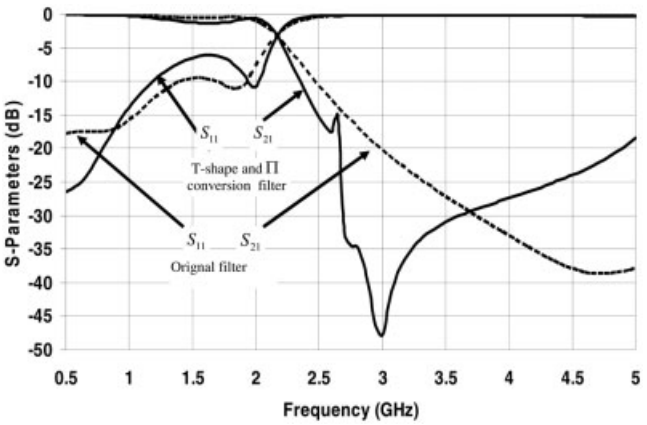

Figure 8 The simulated S-parameters for the original stepped impedance low pass Chebyshev filter and its T-shaped and Π-shaped equivalent filters

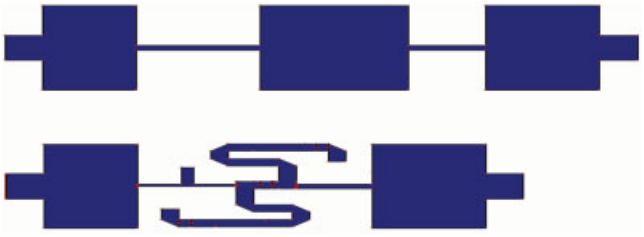

Figure 9 The realized Chebyshev filters (original and the modified geometries). [Color figure can be viewed in the online issue, which is available at www.interscience.wiley.com]

6. FABRICATION AND MEASUREMENTS

The Chebyshev filter and the modified one with the T- and Π-sections that are designed in the previous section are fabricated. Since, the lengths of the shunt transmission lines for the Π-section are taller, they can be easily zigzagged to keep their size less than the widths of the small impedance sections. Also, to prevent the crossing with the filter sections, the zigzagged sections are kept in opposite sides as shown in Figure 9. The S-parameters for both realized filters are measured using a Vector Network Analyzer. A comparison between the simulated S-parameters with the measured results for the original filter structure is shown in Figure 10. From the results, a shift of 0.09 GHz is noticed between the simulated and the measured results. This is probably due to mismatch between the filter edges and the connector that used for measurements and usually is not taken into consideration during the simulation. In general the shift from the designed cutoff frequency (2.25 GHz) for both of the simulated and measured S-parameters is around 45 MHz. Figure 11 illustrates the simulated and measured results for the modified (reduced size) filter. They are similar except for the shift in frequency as in the case of original filter. Small harmonics appear in the simulated and the measured results around 2.75 GHz for the transmission coefficient S_{21} but the response is maintained less than −12 dB around these harmonics. This harmonics is contributed by the coupling of the Π shunt transmission lines with the sections of the filter. The measurement of the S-parameters for both the original and the modified Chebyshev Filters are shown in Figure 12. They have the same response and no shift in the cutoff frequency appears. Good agreement between the measurement results for both filters is demonstrated.

7. CONCLUSIONS

Reductions in the overall size of the stepped impedance filter can be achieved by transferring high impedance line sections into

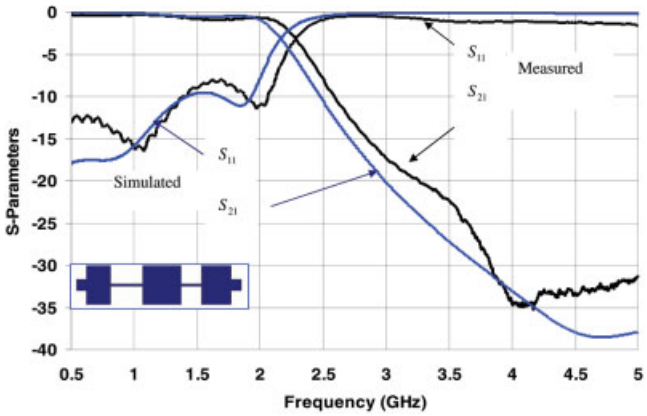

Figure 10 The simulated and the measured S-parameters for the original Chebyshev filter. [Color figure can be viewed in the online issue, which is available at www.interscience.wiley.com]

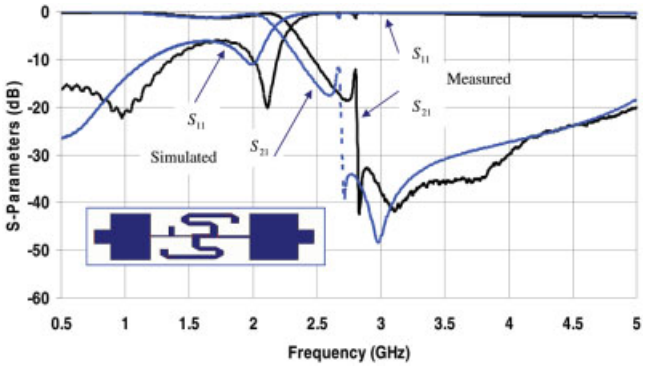

Figure 11 The simulated and the measured S-parameters for the modified (reduced size) Chebyshev filter. [Color figure can be viewed in the online issue, which is available at www.interscience.wiley.com]

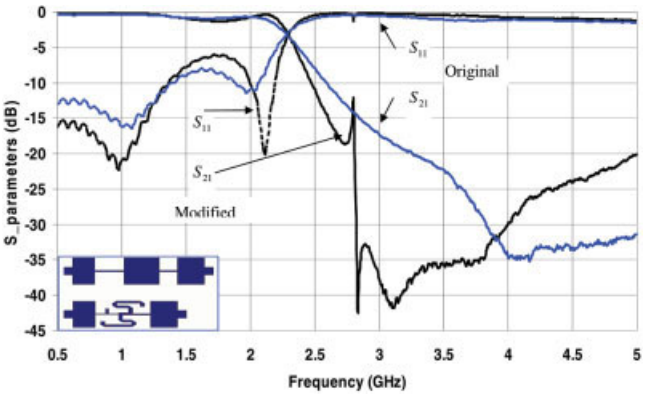

Figure 12 The measured S-parameters for the original and the modified (reduced size) Chebyshev filter. [Color figure can be viewed in the online issue, which is available at www.interscience.wiley.com]

T-sections and low impedance line sections into Π-sections. The design equations for such conversion are given in this article. The reduction in the presented design case is around 25% for moderate five-section Chebyshev low pass filter. When the number of stepped impedance sections is large, as required in sharp response filters, the proposed reduction method will give a substantial size reduction. The designed Chebyshev filter and its (reduced size) equivalent were realized and their S-parameters are measured. Extremely good agreement between the simulated and the measured results is demonstrated.

REFERENCES

1. W.H. Tu and K. Chang, Compact second harmonic-suppressed bandstop and bandpass filters using open stubs, IEEE Trans Microwave Theory Tech 54 (2006), 2497–2502.
2. A.F. Sheta, A. Mohra, and S. Mahmoud, A new class of miniature quadrature couplers for MIC and MMIC applications, Microwave Opt Technol Lett 34 (2002), 215–219.
3. J.S. Hong and M. J. Lancaster, Microstrip filters for RF/microwave applications, Wiley, New York, 2001.
4. D.M. Pozar, Microwave engineering, 3rd ed., Wiley, New York, 2005.
5. Zeland Software Inc. IE3D Software Package, Version 9.35, Zeland Software Inc, 2002.

ALL OPTICAL LINEARIZATION TECHNIQUE OF DFB-LD BASED ON OPTICAL INJECTION LOCKING FOR RoF SYSTEM

Moon-Ki Hong and Sang-Kook Han
Department of Electrical and Electronic Engineering, Yonsei University, Shinchon-Dong, Seodaemoon-Ku, Seoul 120-749, Korea; Corresponding author: skhan@yonsei.ac.kr

Received 8 March 2007

ABSTRACT: *A novel all optical linearization technique using optical injection locking is proposed for radio-over-fiber system. When slave laser diode (SLD) is operated under injection locking condition, the modulated optical signals from master laser diode (MLD) are suppressed by residual amplitude modulation suppression. However, these signals are not completely suppressed by imperfection of residual amplitude modulation suppression and remained in the cavity of SLD. By appropriately controlling the phase and amplitude of these signals to have out-of phase and the same magnitude condition compared with those of direct modulated optical signals from SLD, the efficiency of linearization of DFB-LD can be more enhanced by optical cancellation in the SLD. By using the proposed technique, 17 dB enhancement of carrier-to-interference ratio was experimentally achieved up to frequency response of DFB-LD compared with that of free-running case.* © 2007 Wiley Periodicals, Inc. Microwave Opt Technol Lett 49: 2403–2406, 2007; Published online in Wiley InterScience (www.interscience.wiley.com). DOI 10.1002/mop.22800

Key words: *linearization; intermodulation distortion products; optical injection locking; residual AM suppression; optical cancellation*

1. INTRODUCTION

Recently, high-speed, huge capacity of data transmission and convergence of wired and wireless access network have been requested as the rising of both broadband system and an ubiquitous world. To satisfy these requirements, radio-over-fiber (RoF) systems have been adopted to many applications such as cellular-phone system, mobile internet, WLAN, ITS, and so on [1-3]. Subcarrier multiplexing is one of the best solutions to transmit wireless RF signals by carrying on optical carriers in RoF link because of its simplicity, efficiency, and enough bandwidth for delivery of multichannels [4, 5].

However, in subcarrier multiplexing systems, undesired intermodulation distortion (IMD) products can be generated when RF signals are transmitted in RoF link by nonlinear transmitter such as laser diode. When the transmitted signals are detected at receiver, these nonlinear components may degrade system performance as interference noises [6, 7]. Therefore, these unwanted signals must be removed before transmitting for error-free data service. Especially, the 3rd order IMD products need to be suppressed because it is very difficult to filter out these signals from the carrier signals.

The techniques for suppressing these nonlinear products have been proposed by many researchers [8-13]. Optoelectronic method is one of solutions to reduce IMDs by converting optical signal to electrical signal and using these for removing IMDs of optical transmitter [8-10]. This technique is advantageous because of high linearization efficiency. But, a complicated structure and a requirement of additional components and circuits for optoelectric converting process make this technique less favorable. On the other hand, IMDs can be suppressed by using an all-optical method, which is entirely operated in optical domain [11-13]. This technique is very useful because of its structural simplicity, and availability for broadband application. However, relatively low linearization efficiency would be an obstacle for applying this technique to a practical RoF system.